Single-molecule spectroscopy and super-resolution mapping of physicochemical parameters in the living cell

*Megan A. Steves, Changdong He, Ke Xu**

** xuk@berkeley.edu*

Department of Chemistry, University of California, Berkeley, California 94720, United States.

KEYWORDS

multidimensional super-resolution microscopy, single-molecule spectroscopy, functional imaging, intracellular physicochemical parameters, spectral microscopy, spatial mapping

ABSTRACT

By super-localizing the positions of millions of single molecules over many camera frames, a class of super-resolution fluorescence microscopy methods known as single-molecule localization microscopy (SMLM) has revolutionized how we understand subcellular structures over the past decade. In this review, we highlight emerging studies that transcend the outstanding structural (shape) information offered by SMLM to extract and map physicochemical parameters in the living mammalian cell at single-molecule and super-resolution levels. By encoding-decoding high-dimensional information such as emission and excitation spectra, motion, polarization, fluorescence lifetime, and beyond, for every molecule, and mass-accumulating these measurements for millions of molecules, such multidimensional and multifunctional super-resolution approaches open new windows to intracellular architectures and dynamics, as well as their underlying biophysical rules, far beyond the diffraction limit.

1. Introduction

Recent advances in super-resolution fluorescence microscopy (SRM) based on the massive accumulation of the super-localized positions of single molecules that stochastically switch between emitting and dark states over different camera frames, *i.e.*, single-molecule localization microscopy (SMLM), have led to exciting scientific discoveries and technical developments (1-6). Many existing reviews on SMLM and SRM focus on the ever-increasing spatiotemporal resolutions, aiming to elucidate subcellular structural (shape) information to the best possible extent.

In this review, we focus on emerging work that transcends the outstanding structural information offered by SMLM to extract and map functional (7) physicochemical parameters in the living mammalian cell at single-molecule and super-resolution levels. While such experiments are often enabled by encoding-decoding new dimensions of single-molecule signal, they are also distinct from earlier single-

molecule studies in which isolated events are recorded (8-11). Instead, to achieve mapping at the nanoscale, single-molecule spectroscopies of various forms are mass-accumulated, often for millions of individual molecules, to be integrated with the super-localized positions of the same molecules. Below we categorize our discussion by the different single-molecule signal spaces being probed, including fluorescence intensity, spectra, motion, polarization, lifetime, and non-fluorescence methods. Together, these rising multidimensional SRM approaches afford rich spatial and functional information and hence exciting new insights into the dynamic processes and behaviors of the living cell.

2. Single-molecule fluorescence intensity

Fluorescence intensity remains the most straightforward parameter to analyze in single-molecule data. However, owing to the inherently large molecule-to-molecule variation in emission intensity in SMLM, small changes in intensity are difficult to discriminate. Fluorescence turn-on of initially dark probes offers a strategy to map physical parameters or chemical activities by counting the locally activated molecules. Still, such approaches leave ambiguities between the local level of activation and concentration of probes, hence a blurred boundary between functional and structural readouts. This issue may be overcome with fluorescence spectrum and lifetime detections, which are discussed later in Sections 3 and 6.

2.1. Fluorescence turn-on owing to specific local environments and protein conformations

A class of fluorogenic probes turn on when entering specific physical environments (12). For example, the solvatochromic dye Nile Red is non-fluorescent in aqueous solutions but becomes highly emitting in hydrophobic environments. This effect provides a mechanism in which dynamic single-molecule fluorescence on-off switching is maintained over long periods as probe molecules stochastically enter and exit the hydrophobic phase (**Figure 1a**), hence enabling SMLM for *in vitro* and cellular lipid membranes (**Figure 1b**) (13-16) and *in vitro* protein aggregates (15; 17-19). The fluorescence quantum yield of rotatable molecules can be strongly enhanced by conformation locking. For functional SMLM, such effects have enabled the detection and SRM imaging of specific protein conformations, *e.g.*, β-sheet aggregates in amyloid fibrils (19-24). Beyond the passive binding of fluorogenic probes, Liu *et al.* devised biosensors in which, upon protein conformation changes, a concealed small tag is exposed to bind with a fluorescent reporter. They thus detected single active proteins and tracked their motion in the live-cell plasma membrane (25).

2.2. Reaction-triggered fluorescence turn-on

Initially caged or quenched fluorophores may be turned on by chemical or enzymatic reactions (26), thus opening a window into local activities. For SMLM, Halabi *et al.* devised a fluorogenic probe that was activated by carboxylesterases (**Figure 1c**), and thus reconstructed SRM images of esterase activity in live cells (**Figure 1d**) (27). Chai *et al.* developed a β-galactosidase (β-Gal)-responsive photochromic fluorescent probe, enabling SMLM mapping of the subcellular distribution of β-Gal activity (28).

Fluorophore intensity may also be modulated by ion binding-unbinding. Fluorescent indicators have thus been employed to visualize local bursts of pH and Ca^{2+} signals in live cells. Treating individual

bursts, presumably owing to the collective responses of indicator molecules to individual sub-diffraction-limit events, *e.g.*, synaptic vesicle activities, analogous to single-molecule images in SMLM, thus allowed the super-resolution visualization of activity hotspots (29-31).

2.3. Fluorescence turn-on and fluctuation *via* interactions between biomolecules

Fluorescence turn-on and fluctuation may also be engineered *via* interactions between biomolecules. Based on the tension-induced unzipping of DNA structures, two recent studies employed fluorescent probes that were activated by the piconewton traction forces between single integrin proteins at the cell surface and the substrate, and so achieved SMLM force mapping (*e.g.,* **Figure 1ef**) (32; 33). With split fluorescent proteins (FPs), bimolecular fluorescence complementation (BiFC) has been successfully integrated with SMLM to map protein-protein interactions in live cells (34; 35). Meanwhile, fluorescence fluctuation increase by contact (FLINC) capitalizes on the elevated fluctuations in fluorescence intensity when two FPs are brought into proximity, thus achieving SRM of enzyme activities in live cells (36; 37).

3. Single-molecule spectral responses

Spectral responses provide a robust way to encode functional information that is decoupled from the fluorescence intensity and count of single molecules. Although it has been technically demanding to extract the spectral characteristics of single molecules, recent years have seen the emergence of new approaches that well suit the unique operational schemes of SMLM.

3.1. Wavelength-split detection

A facile method to detect single-molecule spectral responses is wavelength-split detection, in which a dichroic mirror splits (wide-field) fluorescence into two views for the separate, parallel recording of long- and short-wavelength components (**Figure 2a**). For SMLM, this approach enables the identification of single molecules based on the ratio of the detected photon counts in the two views (**Figure 2b**). With a single excitation laser, multicolor SMLM is thus concurrently performed for 2-4 fluorophores of overlapping spectra (*e.g.*, **Figure 2c**) (38-40). For imaging functional parameters, local pH has been examined in gel and silica systems through the two-wavelength ratiometric single-molecule detection of SNARF-1, a fluorescent pH indicator that exhibits substantially different emission spectra in its protonated and deprotonated states, so far limited to sparse molecules (41; 42).

Wavelength-split detection schemes have also been vital to Förster resonance energy transfer (FRET) experiments, in which the relative emission intensities of donor and acceptor fluorophores serve as a molecular ruler for quantifying interactions and conformational dynamics at sub-10 nm length scales (43; 44). Chemically synthesized and genetically encoded FRET-based biosensors have elucidated vital functional parameters inside the living cell, including ion and small-molecule concentrations, cellular microenvironments, and enzymatic activities (45; 46).

Single-molecule FRET (smFRET) offers powerful insights into parameters obscured in ensemble averaging, *e.g.*, multiple states and their interconversions, and so has become an indispensable tool for studying biomolecular conformations and dynamics *in vitro* (44; 47; 48). However, smFRET has seen

limited applications in live cells (44; 49). The relatively low brightness and large size of fluorescent proteins make them unfavorable for smFRET; various approaches have thus been devised to introduce organic dye-based smFRET probes into mammalian and bacterial cells, including microinjection (50-52), heat shock (53), and electroporation (54), or combining FPs with self-labeling tags and fluorogenic membrane-permeable dyes (55). Separately, dye tagging can be more readily achieved for targets at the cell surface (56-58).

With the labeling issues addressed, live-cell smFRET is so far still limited in spatial mapping capabilities. For example, the formation of SNARE protein complexes in the live cell has been examined with wide-field smFRET, but only for ~100 sparsely distributed molecules (51). With confocal smFRET, Konig *et al.* monitored the compaction of the intrinsically disorder protein ProTα in live cells, but only discussed limited spatial information by distinguishing molecules located in the nucleus, cytosol, and outside the cell (52). For studying the dimerization of G protein-coupled receptors (GPCRs) at the cell surface, Asher *et al.* recorded long time traces to monitor dimer conformations and intra-membrane diffusion, but under either low expression levels or after photobleaching to ensure sparse single molecules (58). Utilizing the dynamic binding-unbinding of epidermal growth factor (EGF) labeled by donor or acceptor dyes to EGF receptors (EGFRs) at the cell surface, Winckler *et al.* recorded high-density smFRET in the wide field over ~10^4 frames, and so obtained SMLM maps of EGFR dimers, showing preferential localization to the cell edge (**Figure 2d**) (57). However, quantification of such smFRET data is difficult, as the stochastic labeling leads to only a small proportion of the dimers containing both the donor and acceptor dyes.

3.2. Spectrally resolved SMLM

Although wavelength-split detection is simple in implementation, it achieves limited spectral sensitivity. The ratiometric readouts calculated from the two split views depend on the spectral characteristics of the dichroic mirror used, and so are difficult to compare between studies and vulnerable to operational conditions, including backgrounds.

To resolve the actual emission spectra of single molecules, typical approaches spatially confine the illumination and/or detection (*e.g.*, to a single spot in a confocal setting) to ensure fluorescence is spectrally dispersed from only one single molecule at a time (9; 59). Scanning across the sample then maps out the spectra of different molecules. Although good spectra are recorded, such single-spot detection schemes afford low throughput and limit samples to sparse molecules that are resolvable with diffraction-limited optics.

These limitations are overcome by a new detection scheme in which single-molecule fluorescence is dispersed in the wide field (60; 61). For molecules sparsely distributed in each frame, as encountered in SMLM, it is noted that their images are self-confined into individual emission spots. Concurrent spectral dispersion of these point sources in the wide field thus enables the parallel recording of tens of single-molecule spectra with a ~10 ms camera snapshot (**Figure 3ab**). Next, utilizing single-molecule fluorescence on-off switching to visit different molecules over consecutive camera frames, a key strategy

of SMLM, the spectra of millions of single molecules are thus acquired in minutes, hence affording ultrahigh-throughput single-molecule spectroscopy.

The massively accumulated single-molecule spectra, alongside the concurrently super-localized positions of the same molecules, are synthesized into spectrally resolved SMLM (SR-SMLM) data affording local emission spectra at nanoscale spatial resolution (15; 60-63). When applied to multiplexed imaging (60; 62-64), such approaches achieved crosstalk-free three-dimensional (3D) SRM for four fluorophores with heavily overlapping spectra (60) and the simultaneous tracking of different single molecules and quantum dots (64; 65).

Integration with fluorescent probes that exhibit spectral changes in response to local physicochemical parameters next enabled super-resolution functional mapping. With the solvatochromic dye Nile Red, SR-SMLM thus resolved nanoscale heterogeneities in the membranes of live mammalian cells, showing the intracellular organelle membranes as chemically more polar than the plasm membrane owing to less ordered lipid packing (**Figure 3cd**), and noting the formation of low-polarity, raft-like nanodomains in the plasma membrane upon cholesterol addition or cholera-toxin treatment (16). For *in vitro* systems, Nile Red-based SR-SMLM has similarly resolved chemical polarities for model lipid bilayer membranes and vesicles (15; 16; 66), protein aggregates (**Figure 3ef**) (15; 17; 19), surface adlayers (67), and polymeric nanoparticles (68). A tailor-made Nile Red derivative further enabled the specific probing of the live-cell plasma membrane, unveiling nanoscopic protrusions and invaginations of reduced lipid order (**Figure 3g**) (69). Future SR-SMLM developments may harness the genetic targeting of Nile Red (70; 71) to probe specific subcellular targets.

3.3. Excitation-based spectral imaging

Although spectral fluorescence microscopy methods (72; 73), including SR-SMLM, provide powerful paths toward multiplexed and functional imaging, typical approaches of dispersing the local emission are difficult to implement and limit the time resolution.

Recent work highlights the power of excitation-based spectral microscopy (74-76). By collecting fluorescence with a fixed emission band but scanning the excitation wavelength for the entire imaging field, such schemes remove the need to disperse the emission signal over many detector pixels, as required in typical emission-based spectral microscopy, yet achieve comparable spectral unmixing capabilities. Thus, with camera frame-synchronized fast scanning of the excitation wavelength (**Figure 4a**), six subcellular targets, labeled by fluorophores substantially overlapping in spectrum, were simultaneously imaged in the wide field using a single filter cube at low crosstalk and high speeds (76). Combining different filter cubes enabled multiplexing with more fluorophores (77). The ability to quantify the abundances of different species via the excitation spectra (**Figure 4b**) further enabled the fast, quantitative imaging of intracellular physicochemical parameters, such as pH (**Figure 4c**) and macromolecular crowding, with bi-state and FRET-based biosensors (76).

The application of excitation-based spectral microscopy to SMLM, however, is non-trivial. As the excitation spectrum is collected by monitoring the emission intensity when the excitation wavelength is

scanned, the frequent on-off switching of single-molecule emission in SMLM makes it unreliable, if not impossible, to determine how the emission intensity responses to excitation wavelengths scanned over consecutive camera frames. Wu *et al.* provided an elegant solution in which a resonant mirror rapidly switched the wide-field image back and forth between three recording positions for many rounds within each camera frame (**Figure 4d**) (78). With three synchronized excitation lasers, they thus well discriminated four spectrally overlapped fluorophores for the tetra-color SMLM of fixed cells (**Figure 4e-g**). The potential application of related approaches to living cells and to the functional readouts of fluorescent biosensors presents exciting perspectives.

4. Single-molecule motions

Motions provide yet another great window into molecular behaviors and interactions. Resolving the intracellular movement of biomolecules may enable the spatial mapping of biophysical parameters including diffusion modes and constants, viscosity, binding kinetics, and conformational states (79-86).

4.1. Fluorescence correlation spectroscopy

Fluorescence correlation spectroscopy (FCS) measures fluorescence fluctuations as single molecules transiently enter and leave the detection spot, *e.g.*, in a confocal setting. Through time-correlating the detected fluctuations, FCS provides valuable insights into intracellular diffusions, concentrations, and intermolecular interactions (80; 87; 88). Recent integration with STED (stimulated emission depletion) SRM has further pushed FCS beyond the diffraction limit (89). However, single-molecule events are not isolated, and FCS generally achieves limited spatial mapping capabilities (88; 90).

4.2. Single-particle tracking

To access motions at the true single-molecule level, single-particle tracking (SPT) has found wide use in living cells and been the subject of many reviews (79; 81; 82; 91). Super-localizing single molecules enables motion quantification at the nanoscale. Recent advances in MINFLUX, a method that modulates the illumination pattern to achieve photon-efficient localization of single molecules with exceptional spatiotemporal resolutions (92), have permitted the direct observation of a dye-tagged motor protein stepping on intracellular microtubules with <5 nm spatial resolution at few-millisecond temporal resolutions (93). Monitoring the motion of a single molecule over long trajectories further allows the observation of asynchronous dynamics, *e.g.*, transient intermolecular interactions, and the extraction of diverse biophysical parameters such as binding kinetics, non-Brownian diffusion modes, and directional transport (81; 84).

While SPT is traditionally applied to sparse molecules to avoid trajectory overlapping, recent developments integrating SMLM-inspired photoactivation and fluorophore-exchange schemes have permitted the high-density tracking of single-molecule trajectories (57; 91; 94-97). However, the focus is often on obtaining long trajectories to assign a diffusion coefficient value to each molecule, thus yielding limited spatial mapping and restricting applications to slow diffusion in membranes, where the bound molecules stay in focus over many frames.

4.3. Single-molecule displacement/diffusivity mapping

To overcome SPT's limited spatial mapping capabilities and access the fast diffusion of unbound molecules, an emerging approach, single-molecule displacement/diffusivity mapping (SM*d*M) (98; 99), forgoes trajectories but focuses on transient displacements. Thus, rather than following how each molecule behaves as it randomly visits different, potentially heterogeneous locations, SM*d*M flips the question to survey, for each fixed location, how different (yet identical) single molecules move locally. This location-centered strategy is naturally powerful for spatial mapping. Moreover, by focusing on transient displacements, each molecule only needs to be localized twice within a short time window. For fast-diffusing molecules, a tandem excitation scheme is thus devised to apply a pair of closely timed stroboscopic pulses across two camera frames to capture single-molecule images over time separations substantially shorter than the camera frame time, from which single-molecule displacements are extracted (**Figure 5ab**) (98). This tandem excitation scheme further leaves ample time between the anti-paired pulses (**Figure 5ab**) to allow efficient probe exchanges through diffusion, thus enabling SM*d*M for non-photoswitchable fluorophores (98; 100). Repeating the above scheme ~10^4 times next accumulates millions of single-molecule displacements to be spatially binned for individual fitting to extract local diffusion coefficient D (**Figure 5cd**) and generate its super-resolved map (**Figure 5e**) (98). Local displacement direction analysis is further developed to elucidate diffusion anisotropy (**Figure 5f**) (99; 101).

With ~30 kDa FPs, SM*d*M thus uncovered nanoscale diffusion heterogeneities in the mammalian cytoplasm (**Figure 5e**), nucleus (**Figure 5g**), and organelles, and identified the protein net charge as a key determinant of intracellular diffusion (**Figure 5h**) (98; 101). By squeezing the tandem-pulse time separation to 400 μs and incorporating graphene-based electroporation for probe delivery (102), SM*d*M further quantified the very fast diffusion of small (<1 kDa) solutes, unveiling their unhindered diffusion in the mammalian cell (**Figure 5i**) (100). For cellular membranes, integration of SM*d*M with Nile Red-based SR-SMLM resolved diffusion heterogeneities of different origins (99). For *in vitro* FUS condensates formed through liquid-liquid phase separation, SM*d*M unveiled substantial diffusion slowdowns at surface nanoaggregates (19).

The massively accumulated single-molecule displacements in SM*d*M further enable D-value determination to ±1% precisions (103), which has been utilized to establish a universal dependency of D on molecular weight for proteins and small molecules (102; 103), show no changes in D in enzyme reactions (103), and determine how D scales with meshwork sizes in expandable hydrogels (104).

While SM*d*M of FPs in mammalian cells has so far focused on elucidating nonspecific charge interactions, tagging FPs to specific intracellular proteins could employ SM*d*M to map intracellular protein conformation, oligomerization, and interactions; recent SM*d*M work on bacteria has pointed to such directions (105; 106). The compatibility of SM*d*M with non-photoswitchable fluorophores (98; 100) and the demonstrated successful intracellular probe delivery for SM*d*M (100) further imply the possible integration of SM*d*M with the above-discussed dye-based smFRET for functional readouts. Meanwhile,

while SM*d*M has unveiled rich diffusion heterogeneity by just analyzing single-step displacements between tandem frames, future developments may expand on this concept to enable the detection of few-step short tracks, from which one may garner information on nonlinear diffusion and dynamic transition between states.

5. Single-molecule fluorescence polarization and anisotropy

Fluorescence polarization and anisotropy offer valuable information about molecular orientations and dynamics (107; 108). Splitting the fluorescence emission into orthogonal polarizations and/or modulating the polarization orientation of the excitation laser enable the encoding-decoding of single-molecule polarization and anisotropy in SMLM (109-112).

Biological filaments are often assembled from oriented subunits. For *in vitro* samples, the fixed binding orientations of fluorogenic probes to filaments have thus yielded clear molecular orientations for DNA strands (111-113) and amyloid fibrils (18; 21) in polarization-resolved SMLM data. For imaging in the mammalian cell, early studies examined fluorescence anisotropy in the SMLM data of FP-tagged actin to detect local heterogeneity in rotational mobility (109; 110). Valades Cruz *et al.* compared polarization-resolved SMLM data for differently labeled microtubule and actin cytoskeletons in fixed cells, and identified Alexa Fluor 488-phalloidin as a good probe to resolve the orientation of the latter (112). By delivering the same probe into live mammalian cells at low concentrations, Mehta *et al.* resolved actin filament orientations in SPT to compare with the retrograde flow direction at the leading edge (114). Rimoli *et al.* recently developed strategies to determine single molecules' orientation in 2D and infer their 3D orientations, which they applied to the SMLM of Alexa Fluor 488-phalloidin-labeled dense actin structures in fixed cells (**Figure 6a-d**) (115).

Polarization-based functional SMLM has also shed new light on the structure of lipid membranes. Integrating polarized beam-splitting and a spatial light modulator, Lu *et el.* encoded 3D orientation and wobbling into the single-molecule point spread function, and thus analyzed the ordering and packing effects of cholesterol in supported lipid bilayers and resolved nanoscale domains with different ordering parameters (116). A recent study constructed a radially and azimuthally polarized multi-view reflector to image single-molecule fluorescence across eight polarization channels to simultaneously determine molecular location and orientation in three dimensions each, and the resultant 6D SMLM resolved dye orientations in fixed-cell membranes (**Figure 6e-f**) (117).

6. Single-molecule fluorescence lifetime

By detecting the exponential decay rate of emission at the nanosecond time scale, fluorescence lifetime imaging microscopy (FLIM) provides a powerful, probe concentration-insensitive handle for the functional imaging of biological samples (118-120), with diverse probes developed for chemical polarity, viscosity, temperature, and different analytes.

Fluorescence lifetime-resolved SMLM (FL-SMLM) has been achieved with both confocal and wide-field experimental setups (**Figure 7a-d**), utilizing a single-element single-photon avalanche diode

detector or an array detector based on a microchannel-plate photomultiplier tube, respectively (121; 122). Whereas confocal setups can only image a relatively small field of view with reasonable imaging speeds, the currently available array detectors suffer from low (~5%) quantum efficiencies. Lifetime estimations can also be made for the wide field with conventional high-sensitivity cameras by time-gating the signal electro-optically with a Pockels cell (**Figure 7ef**) (123), but with limitations on sensitivity.

Thus far, the application of FL-SMLM has been limited to *in vitro* samples and fixed cells, with an initial focus on separating labels for multiplexed imaging (**Figure 7bcf**) (121; 122; 124). Recent work detected FRET (125) and metal/graphene-induced energy transfer (122; 126; 127), the latter further enabling 3D-SMLM by providing an interesting way to determine the fluorophore's distance to the substrate (**Figure 7d**). Possible future FL-SMLM applications to live cells and to the super-resolution mapping of local environments and intermolecular interactions hold great potential.

7. Non-fluorescence methods

The above success of SMLM for functional SRM imaging raises the question of whether related approaches could be applied to non-fluorescence methods, which may overcome the limited number of photons that can be extracted from individual fluorophores, enable label-free imaging, or access new spectroscopy insights for decoding physicochemical parameters (128-130).

Microspheres and nanoparticles have long served as unbleachable probes for live-cell SPT (91; 131). Recent advances in photothermal microscopy (91; 128; 132) and interferometric scattering microscopy (133-136) have further enabled the SPT of small gold nanoparticles in live cells, as well as the room-temperature detection and analysis of single molecules *in vitro*. It, however, remains a challenge to resolve single molecules in the crowded cell, or to detect many molecules within the diffraction limit.

Nonlinear optical methods such as nonlinear Raman, harmonic generation, multiphoton fluorescence, and transient absorption offer intriguing prospects for functional SRM for their outstanding chemical and structural contrasts (130; 137-139). Super-resolution nonlinear optical microscopy has been achieved with expansion microscopy (140; 141), STED-based imaging (142), and interferometric excitation (143), among other approaches (129; 130). Application to SMLM is limited by the relatively low probability of nonlinear optical processes and the need for a scalable approach to signal modulation for the isolation of single molecules. Plasmonic amplification of light-matter interactions (144) provides a viable path; surface-enhanced Raman spectroscopy (SERS) has achieved single-molecule sensitivity (145; 146), and its local blinking has enabled SMLM-type imaging of dried samples (147; 148). However, the patterned plasmonic substrates distort the resultant image, and their required proximity to the sample limits applicability.

8. Conclusion

In conclusion, while the outstanding spatial resolution of SMLM has attracted wide attention, in this review we have showcased how, by extending mass-accumulated single-molecule measurements to higher dimensions, including emission and excitation spectra, motion, polarization, and fluorescence lifetime,

the resultant multidimensional SRM approaches provide fascinating new insights into physicochemical parameters in the living cell.

Future developments call for a synergy of continued innovations in optics on both the excitation and detection fronts, fluorescent probe design, synthesis, and delivery methods, as well as algorithm and analysis tools. The need to detect single molecules and invoke fluorescence on-off switching poses significant challenges: optimal results thus demand bright probes with high fluorescence quantum yields, while on-off mechanisms such as photoswitching or reversible binding often need to be built in. Yet, the uniqueness of sparse molecules across the camera frame, as often achieved in SMLM, offers new possibilities, so that single-molecule images may be directly stretched/dispersed in the wide field for high-throughput recording, and the recorded signal from each molecule is guaranteed a single identity, removing the need of unmixing. New illumination sequences further enable SMLM/SM*d*M for constantly bright fluorophores *via* diffusion-based probe exchange. Integrations between different SMLM modules, as well as correlative approaches with other microscopy and spectroscopy techniques (149), provide additional opportunities.

DISCLOSURE STATEMENT

The authors are not aware of any affiliations, memberships, funding, or financial holdings that might be perceived as affecting the objectivity of this review.

ACKNOWLEDGMENTS

We acknowledge support by the National Institute of General Medical Sciences of the National Institutes of Health (DP2GM132681 and R35GM149349), the National Science Foundation (CHE-2203518), the Packard Fellowships for Science and Engineering, and the Heising-Simons Faculty Fellows Award.

Figure Captions

Figure 1. SMLM *via* fluorescence turn-on from specific local environments, reactions, and engineered biomolecular interactions. (a) Fluorescence intensity time trace for a lipid vesicle, showing bursts due to the stochastic entering of single Nile Red molecules into the lipid phase from the aqueous medium. (b) SMLM image of a supported lipid bilayer obtained by localizing 2,778 single Nile Red molecules over 4,095 frames due to the above fluorescence turn-on process. Panels *a-b* adapted from Reference (13); copyright 2006 National Academy of Sciences. (c) Schematic: A caged (initially dark) probe (**1**) that can be photoactivated into a fluorescent state after removal of the acetyl group by carboxylesterases (**2**). (d) SMLM image of esterase activity based on **1** in a live mammalian cell. Panels *c-d* adapted with permission from Reference (27); copyright 2017 American Chemical Society. (e) Schematic: Cellular force SMLM

based on force-activatable emitters in which the unzipping of a DNA/PNA (peptide nucleic acid) hybrid leads to fluorescence dequenching and single-molecule emission. (f) Resultant integrin molecular tension SMLM of a migrating keratocyte from 20 frames of recording. Panels *e-f* adapted with permission from Reference (32); copyright 2020 American Chemical Society.

Figure 2. Split-wavelength detection for multicolor SMLM and smFRET in living cells. (a) Schematic: A dichroic mirror (DCM) separates long- and short-wavelength components of single-molecule emission for simultaneous imaging on two areas of a CCD. (b) Distribution of photon counts in the long- and short-wavelength channels for single molecules detected in SMLM, for four dyes with overlapping emission spectra (inset) (c) Simultaneous four-color SMLM of a fixed cell by separating the single-molecule emission of four dyes based on *b*. Panels *b-c* adapted with permission from Reference (39); copyright 2010 Elsevier. (d) SMLM images due to the binding-unbinding of a mixture of donor- and acceptor-labeled EGF molecules to EGFR in the plasma membrane of a live mammalian cell, for the donor (top) and acceptor (bottom) channels when exciting the donor. Insets: Zoom-ins of the boxed regions. Single-molecule emission in the acceptor channel is attributed to smFRET between single donor- and acceptor-labeled EGFs bound to an EGFR dimer. Panel *d* adapted from Reference (57) (CC BY-NC-ND).

Figure 3. SR-SMLM and super-resolution mapping of chemical polarity for live-cell membranes and *in vitro* protein aggregates. (a) Schematic: Fluorescence is dispersed in the wide field, so the emission spectra of many single molecules are concurrently captured in a camera frame. Single-molecule fluorescence on-off switching next enables the sampling of different molecules over consecutive frames. (b) Example spectra of single Alexa Fluor 647 molecules recorded in a 9-ms camera frame. Panel *b* adapted from Reference (60). (c) SR-SMLM image of Nile Red-highlighted lipid-membrane system in a live mammalian cell. Color presents the single-molecule spectral mean; longer emission wavelengths correspond to higher local chemical polarities. (d) Averaged single-molecule spectra at the plasma membrane versus the internal nanoscale organelle membranes, compared to that at supported lipid bilayers with and without the packing-order promoter cholesterol (Chol). Panels *c-d* adapted with permission from Reference (16); copyright 2017 American Chemical Society. (e) SR-SMLM images of Nile Red at the surfaces of *in vitro* amyloid-β oligomers (left) and fibrils (right). (f) Frequency histogram of fluorescence emission peaks for individual Nile Red molecules at the amyloid-β oligomers and fibrils. Panels *e-f* adapted from Reference (15) (CC BY). (g) SR-SMLM image for the plasma membrane of a live mammalian cell labeled by NR4A, a Nile Red derivative. Arrows point to higher local chemical polarities at endocytic sites due to reduced lipid order. Panel *g* adapted with permission from Reference (69).

Figure 4. Excitation-based spectral microscopy and application to SMLM. (a) Schematic: the excitation wavelength is varied in consecutive frames through the frame-synchronized modulation of the acousto-optic tunable filter (AOTF). P polarizer, L lens, F bandpass filter, DM dichroic mirror. (b) 8-wavelength excitation spectrum recorded with the setup in *a*, for pHRed FP expressed in a mammalian cell that was

equilibrated to pH = 8.0 (black solid line), and its linear unmixing into the deprotonated (A^-) and protonated (HA) components (dash lines). (c) Color-coded absolute pH map series for pHRed expressed in the mitochondrial matrix in a living mammalian cell, as obtained through the linear unmixing of the excitation spectrum as in *b*, showing concurrent fast changes in both the mitochondrial shape and matrix pH at 0.8 s time resolution. Panels *a-c* adapted from Reference (76) (CC BY 4.0). (d) Schematic for excitation-resolved SMLM: A resonant mirror fast-switches the wide-field image back and forth between three recording positions with synchronized excitation of three lasers of different wavelengths. (e) Scatter plot of the photon counts for individual Alexa Fluor 647 molecules when excited by the three lasers. (f) Tetra-color SMLM by separating the excitation characteristics of four dyes based on their three-excitation-wavelength single-molecule photon counts as shown in *e*. (g) Separated channels for the box in *f*, showing minimal crosstalk. Panels *d-g* adapted from Reference (78) (CC BY 4.0).

Figure 5. SM*d*M: Super-resolution mapping of fast intracellular diffusion. (a) Schematic: A pair of closely timed stroboscopic excitation pulses are applied across two tandem camera frames, so that the two recorded images correspond to the short time separation Δt between the paired pulses. This paired excitation scheme is repeated ~10^4 times to enable statistics. (b) Example single-molecule images of sulforhodamine-101 molecules diffusing in a living rat astrocyte, recorded in four consecutive frames with the above tandem excitation scheme. Here, each pulse lasted 200 μs, the center-to-center separation between paired pulses was Δt = 500 μs, and the camera frame time was 9.15 ms. Insets: comparison of the localized single-molecule positions across the tandem frames, from which single-molecule displacements are extracted. Panel *b* adapted with permission from Reference (100); copyright 2023 American Chemical Society. (c,d) Distributions of displacements in Δt =1 ms for single mEos3.2 FP molecules in a living mammalian cell, for two adjacent 300×300 nm^2 areas marked with orange and red boxes in *e*. Blue curves: fits to a diffusion model, with resultant *D* values labeled. (e) Color-coded SM*d*M *D* map for the intracellular diffusion of mEos3.2, obtained by spatially binning the accumulated single-molecule displacements onto 100 × 100 nm^2 grids for local fitting as in *c,d*. Panels *c-e* adapted from Reference (98). (f) Color map presenting the SM*d*M-determined local principal direction of diffusion for BDP-TMR-alkyne in cellular membranes, showing anisotropic diffusion along the endoplasmic-reticulum tubules. Panel *f* adapted with permission from Reference (99) ; copyright 2020 American Chemical Society. (g) SM*d*M *D* map for mEos3.2 FP in the nuclear region of a living mammalian cell (left) versus SMLM of the same region with a DNA stain (right), showing reduced *D* in the nucleolus (asterisk) and fast and slow diffusion regions correlating to low and high local DNA densities (red and orange arrows). (h) SM*d*M-determined mean *D* values for mEos3.2 FPs of different net charges in different subcellular environments. Panels *g-h* adapted from Reference (98). (i) SM*d*M *D* map of Cy3B dye in a living mammalian cell, obtained with Δt =400 μs. Panel *i* adapted with permission from Reference (100); copyright 2023 American Chemical Society.

Figure 6. Polarization-resolved SMLM and its applications to cytoskeleton and membrane in fixed cells. (a) Schematic: fluorescence polarization behavior of Alexa Fluor 488-phalloidin labeling an actin filament.

(b) Schematic: extracting single-molecule fluorescence polarization orientation and wobbling by combining a half-wave plate (HWP) and two polarizing beamsplitters (PBS) and applying diaphragms (D) to reduce the detection numerical aperture. (c-d) Resultant SMLM images resolving the mean orientation (c) and wobbling angle (d) of Alexa Fluor 488-phalloidin labeling the actin cytoskeleton in a fixed cell. Panels *a-d* adapted from Reference (115) (CC BY). (e,f) 6D (3D spatial and 3D orientational) SMLM imaging of merocyanine 540 molecules bound to the membrane of a fixed cell: (e) In plane (*x*-*y*) view, colored by the single-molecule azimuthal angle ϕ. (f) Vertical (*y*-*z*) view of the boxed region, colored by the single-molecule polar angle θ. Panels *e-f* adapted with permission from Reference (117).

Figure 7. Fluorescence lifetime-resolved SMLM. (a) Comparison of the fluorescence lifetime of single molecules of five dyes measured with confocal and wide-field SMLM setups. (b) Top: Wide-field lifetime-resolved SMLM image of a fixed cell double labeled with Cy3B against peroxisomes and Atto 550 against mitochondria, with color presenting the measured lifetime. Bottom: Zoom-in of the boxed region and separation of the two dyes based on lifetime. (c) Lifetime histograms corresponding to *b*. Panels *a-c* adapted from Reference (122) (CC-BY-NC-ND 4.0). (d) Fluorescence lifetime curves for AF647-DNA molecules on glass and on gold substrates with 10-50 nm thick SiO_2 spacers measured with confocal lifetime imaging, demonstrating distance-dependence decreases in fluorescence lifetime owing to metal-induced energy transfer. Panel *d* adapted from Reference (126) (CC BY-NC). (e) Schematic: Time-gated electro-optic imaging for wide-field lifetime-resolved SMLM using a resonantly driven Pockels cell and a polarizing beamsplitter. (f) Resultant lifetime-resolved SMLM image of DNA origamis labeled with Cy3B and Atto 565. Panels *e,f* adapted with permission from Reference (123); copyright 2021 American Chemical Society.

LITERATURE CITED

1. Liu Z, Lavis LD, Betzig E. 2015. Imaging live-cell dynamics and structure at the single-molecule level. *Mol. Cell* 58:644-59
2. Sahl SJ, Hell SW, Jakobs S. 2017. Fluorescence nanoscopy in cell biology. *Nat. Rev. Mol. Cell Biol.* 18:685-701
3. Sigal YM, Zhou R, Zhuang X. 2018. Visualizing and discovering cellular structures with super-resolution microscopy. *Science* 361:880-7
4. Möckl L, Moerner WE. 2020. Super-resolution microscopy with single molecules in biology and beyond-essentials, current trends, and future challenges. *J. Am. Chem. Soc.* 142:17828-44
5. Lelek M, Gyparaki MT, Beliu G, Schueder F, Griffié J, et al. 2021. Single-molecule localization microscopy. *Nat. Rev. Methods Primers* 1:39
6. Xiang L, Chen K, Xu K. 2021. Single molecules are your quanta: A bottom-up approach toward multidimensional super-resolution microscopy. *ACS Nano* 15:12483-96
7. Yan R, Wang B, Xu K. 2019. *Functional* super-resolution microscopy of the cell. *Curr. Opin. Chem. Biol.* 51:92-7
8. Weiss S. 1999. Fluorescence spectroscopy of single biomolecules. *Science* 283:1676-83
9. Moerner WE, Fromm DP. 2003. Methods of single-molecule fluorescence spectroscopy and microscopy. *Rev. Sci. Instrum.* 74:3597-619

10. Xie XS, Choi PJ, Li GW, Lee NK, Lia G. 2008. Single-molecule approach to molecular biology in living bacterial cells. *Ann. Rev. Biophys.* 37:417-44
11. Joo C, Balci H, Ishitsuka Y, Buranachai C, Ha T. 2008. Advances in single-molecule fluorescence methods for molecular biology. *Annu. Rev. Biochem.* 77:51-76
12. Klymchenko AS. 2017. Solvatochromic and fluorogenic dyes as environment-sensitive probes: design and biological applications. *Acc. Chem. Res.* 50:366-75
13. Sharonov A, Hochstrasser RM. 2006. Wide-field subdiffraction imaging by accumulated binding of diffusing probes. *Proc. Natl. Acad. Sci. U. S. A.* 103:18911-6
14. Lew MD, Lee SF, Ptacin JL, Lee MK, Twieg RJ, et al. 2011. Three-dimensional superresolution colocalization of intracellular protein superstructures and the cell surface in live *Caulobacter crescentus*. *Proc. Natl. Acad. Sci. U. S. A.* 108:E1102-E10
15. Bongiovanni MN, Godet J, Horrocks MH, Tosatto L, Carr AR, et al. 2016. Multi-dimensional super-resolution imaging enables surface hydrophobicity mapping. *Nat Commun* 7:13544
16. Moon S, Yan R, Kenny SJ, Shyu Y, Xiang L, et al. 2017. Spectrally resolved, functional super-resolution microscopy reveals nanoscale compositional heterogeneity in live-cell membranes. *J. Am. Chem. Soc.* 139:10944-7
17. Lee JE, Sang JC, Rodrigues M, Carr AR, Horrocks MH, et al. 2018. Mapping surface hydrophobicity of α-synuclein oligomers at the nanoscale. *Nano Lett.* 18:7494-501
18. Ding T, Wu T, Mazidi H, Zhang O, Lew MD. 2020. Single-molecule orientation localization microscopy for resolving structural heterogeneities between amyloid fibrils. *Optica* 7:602-7
19. He C, Wu CY, Li W, Xu K. 2023. Multidimensional super-resolution microscopy unveils nanoscale surface aggregates in the aging of FUS condensates. *J. Am. Chem. Soc.*:DOI: 10.1021/jacs.3c08674
20. Ries J, Udayar V, Soragni A, Hornemann S, Nilsson KP, et al. 2013. Superresolution imaging of amyloid fibrils with binding-activated probes. *ACS Chem Neurosci* 4:1057-61
21. Shaban HA, Valades-Cruz CA, Savatier J, Brasselet S. 2017. Polarized super-resolution structural imaging inside amyloid fibrils using Thioflavine T. *Sci. Rep.* 7:12482
22. Needham LM, Weber J, Varela JA, Fyfe JWB, Do DT, et al. 2020. ThX - a next-generation probe for the early detection of amyloid aggregates. *Chem Sci* 11:4578-83
23. Torra J, Viela F, Megias D, Sot B, Flors C. 2022. Versatile Near-Infrared Super-Resolution Imaging of Amyloid Fibrils with the Fluorogenic Probe CRANAD-2. *Chem. Eur. J.* 28:e202200026
24. Morten MJ, Sirvio L, Rupawala H, Mee Hayes E, Franco A, et al. 2022. Quantitative super-resolution imaging of pathological aggregates reveals distinct toxicity profiles in different synucleinopathies. *Proc Natl Acad Sci U S A* 119:e2205591119
25. Liu B, Stone OJ, Pablo M, Herron JC, Nogueira AT, et al. 2021. Biosensors based on peptide exposure show single molecule conformations in live cells. *Cell* 184:5670-85
26. Chan J, Dodani SC, Chang CJ. 2012. Reaction-based small-molecule fluorescent probes for chemoselective bioimaging. *Nat Chem* 4:973-84
27. Halabi EA, Thiel Z, Trapp N, Pinotsi D, Rivera-Fuentes P. 2017. A Photoactivatable Probe for Super-Resolution Imaging of Enzymatic Activity in Live Cells. *J Am Chem Soc* 139:13200-7
28. Chai X, Han HH, Sedgwick AC, Li N, Zang Y, et al. 2020. Photochromic Fluorescent Probe Strategy for the Super-resolution Imaging of Biologically Important Biomarkers. *J Am Chem Soc* 142:18005-13
29. Tang AH, Chen H, Li TP, Metzbower SR, MacGillavry HD, Blanpied TA. 2016. A trans-synaptic nanocolumn aligns neurotransmitter release to receptors. *Nature* 536:210-4
30. Ellefsen KL, Holt JR, Chang AC, Nourse JL, Arulmoli J, et al. 2019. Myosin-II mediated traction forces evoke localized Piezo1-dependent Ca^{2+} flickers. *Commun. Biol.* 2:298
31. Newman ZL, Bakshinskaya D, Schultz R, Kenny SJ, Moon S, et al. 2022. Determinants of synapse diversity revealed by super-resolution quantal transmission and active zone imaging. *Nat. Commun.* 13:229
32. Zhao Y, Pal K, Tu Y, Wang X. 2020. Cellular force nanoscopy with 50 nm resolution based on integrin molecular tension imaging and localization. *J. Am. Chem. Soc.* 142:6930-4

33. Brockman JM, Su H, Blanchard AT, Duan Y, Meyer T, et al. 2020. Live-cell super-resolved PAINT imaging of piconewton cellular traction forces. *Nat. Methods* 17:1018-24
34. Nickerson A, Huang T, Lin LJ, Nan X. 2014. Photoactivated localization microscopy with bimolecular fluorescence complementation (BiFC-PALM) for nanoscale imaging of protein-protein interactions in cells. *PLoS One* 9:e100589
35. Liu Z, Xing D, Su QP, Zhu Y, Zhang J, et al. 2014. Super-resolution imaging and tracking of protein-protein interactions in sub-diffraction cellular space. *Nat. Commun.* 5:4443
36. Mo GCH, Ross B, Hertel F, Manna P, Yang XX, et al. 2017. Genetically encoded biosensors for visualizing live-cell biochemical activity at super-resolution. *Nat. Methods* 14:427-34
37. Lin W, Mo GCH, Mehta S, Zhang J. 2021. DrFLINC Contextualizes Super-resolution Activity Imaging. *J. Am. Chem. Soc.* 143:14951-5
38. Bossi M, Folling J, Belov VN, Boyarskiy VP, Medda R, et al. 2008. Multicolor far-field fluorescence nanoscopy through isolated detection of distinct molecular species. *Nano Lett.* 8:2463-8
39. Testa I, Wurm CA, Medda R, Rothermel E, von Middendorf C, et al. 2010. Multicolor fluorescence nanoscopy in fixed and living cells by exciting conventional fluorophores with a single wavelength. *Biophys. J.* 99:2686-94
40. Gunewardene MS, Subach FV, Gould TJ, Penoncello GP, Gudheti MV, et al. 2011. Superresolution imaging of multiple fluorescent proteins with highly overlapping emission spectra in living cells. *Biophys. J.* 101:1522-8
41. Brasselet S, Moerner WE. 2000. Fluorescence behavior of single-molecule pH-sensors. *Single Molecules* 1:17-23
42. Sun X, Xie J, Xu J, Higgins DA, Hohn KL. 2015. Single-molecule studies of acidity distributions in mesoporous aluminosilicate thin films. *Langmuir* 31:5667-75
43. Algar WR, Hildebrandt N, Vogel SS, Medintz IL. 2019. FRET as a biomolecular research tool - understanding its potential while avoiding pitfalls. *Nat. Methods* 16:815-29
44. Lerner E, Barth A, Hendrix J, Ambrose B, Birkedal V, et al. 2021. FRET-based dynamic structural biology: Challenges, perspectives and an appeal for open-science practices. *eLife* 10:e60416
45. Greenwald EC, Mehta S, Zhang J. 2018. Genetically encoded fluorescent biosensors illuminate the spatiotemporal regulation of signaling networks. *Chem. Rev.* 118:11707-94
46. Wu L, Huang C, Emery BP, Sedgwick AC, Bull SD, et al. 2020. Förster resonance energy transfer (FRET)-based small-molecule sensors and imaging agents. *Chemical Society Reviews* 49:5110-39
47. Roy R, Hohng S, Ha T. 2008. A practical guide to single-molecule FRET. *Nat. Methods* 5:507-16
48. Lerner E, Cordes T, Ingargiola A, Alhadid Y, Chung S, et al. 2018. Toward dynamic structural biology: Two decades of single-molecule Förster resonance energy transfer. *Science* 359:eaan1133
49. Sustarsic M, Kapanidis AN. 2015. Taking the ruler to the jungle: single-molecule FRET for understanding biomolecular structure and dynamics in live cells. *Curr. Opin. Struct. Biol.* 34:52-9
50. Murakoshi H, Iino R, Kobayashi T, Fujiwara T, Ohshima C, et al. 2004. Single-molecule imaging analysis of Ras activation in living cells. *Proc. Natl. Acad. Sci. U. S. A.* 101:7317-22
51. Sakon JJ, Weninger KR. 2010. Detecting the conformation of individual proteins in live cells. *Nature Methods* 7:203-5
52. König I, Zarrine-Afsar A, Aznauryan M, Soranno A, Wunderlich B, et al. 2015. Single-molecule spectroscopy of protein conformational dynamics in live eukaryotic cells. *Nature Methods* 12:773-9
53. Fessl T, Adamec F, Polívka T, Foldynová-Trantírková S, Vácha F, Trantírek L. 2012. Towards characterization of DNA structure under physiological conditions in vivo at the single-molecule level using single-pair FRET. *Nucleic Acids Research* 40:e121-e
54. Crawford R, Joseph, Aigrain L, Plochowietz A, Gryte K, et al. 2013. Long-Lived Intracellular Single-Molecule Fluorescence Using Electroporated Molecules. *Biophysical Journal* 105:2439-50
55. Okamoto K, Hibino K, Sako Y. 2020. In-cell single-molecule FRET measurements reveal three conformational state changes in RAF protein. *Biochim Biophys Acta Gen Subj* 1864:129358

56. Sako Y, Minoghchi S, Yanagida T. 2000. Single-molecule imaging of EGFR signalling on the surface of living cells. *Nature Cell Biology* 2:168-72
57. Winckler P, Lartigue L, Giannone G, De Giorgi F, Ichas F, et al. 2013. Identification and super-resolution imaging of ligand-activated receptor dimers in live cells. *Sci. Rep.* 3:2387
58. Asher WB, Geggier P, Holsey MD, Gilmore GT, Pati AK, et al. 2021. Single-molecule FRET imaging of GPCR dimers in living cells. *Nat. Methods* 18:397-405
59. Michalet X, Siegmund OHW, Vallerga JV, Jelinsky P, Millaud JE, Weiss S. 2007. Detectors for single-molecule fluorescence imaging and spectroscopy. *J. Mod. Opt.* 54:239-81
60. Zhang Z, Kenny SJ, Hauser M, Li W, Xu K. 2015. Ultrahigh-throughput single-molecule spectroscopy and spectrally resolved super-resolution microscopy. *Nat. Methods* 12:935-8
61. Yan R, Moon S, Kenny SJ, Xu K. 2018. Spectrally resolved and functional super-resolution microscopy via ultrahigh-throughput single-molecule spectroscopy. *Acc. Chem. Res.* 51:697-705
62. Mlodzianoski MJ, Curthoys NM, Gunewardene MS, Carter S, Hess ST. 2016. Super-resolution imaging of molecular emission spectra and single molecule spectral fluctuations. *PLoS One* 11:e0147506
63. Dong B, Almassalha L, Urban BE, Nguyen TQ, Khuon S, et al. 2016. Super-resolution spectroscopic microscopy via photon localization. *Nat. Commun.* 7:12290
64. Huang T, Phelps C, Wang J, Lin LJ, Bittel A, et al. 2018. Simultaneous multicolor single-molecule tracking with single-laser excitation via spectral imaging. *Biophys. J.* 114:301-10
65. Kakizuka T, Ikezaki K, Kaneshiro J, Fujita H, Watanabe TM, Ichimura T. 2016. Simultaneous nano-tracking of multiple motor proteins via spectral discrimination of quantum dots. *Biomed. Opt. Express.* 7:2475-93
66. Davis JL, Zhang Y, Yi SJ, Du FF, Song KH, et al. 2020. Super-Resolution Imaging of Self-Assembled Nanocarriers Using Quantitative Spectroscopic Analysis for Cluster Extraction. *Langmuir* 36:2291-9
67. Xiang L, Wojcik M, Kenny SJ, Yan R, Moon S, et al. 2018. Optical characterization of surface adlayers and their compositional demixing at the nanoscale. *Nat. Commun.* 9:1435
68. Archontakis E, Deng L, Zijlstra P, Palmans ARA, Albertazzi L. 2022. Spectrally PAINTing a Single Chain Polymeric Nanoparticle at Super-Resolution. *J. Am. Chem. Soc.* 144:23698-707
69. Danylchuk DI, Moon S, Xu K, Klymchenko AS. 2019. Switchable solvatochromic probes for live-cell super-resolution imaging of plasma membrane organization. *Angew. Chem. Int. Ed.* 58:14920-4
70. Prifti E, Reymond L, Umebayashi M, Hovius R, Riezman H, Johnsson K. 2014. A Fluorogenic Probe for SNAP-Tagged Plasma Membrane Proteins Based on the Solvatochromic Molecule Nile Red. *ACS Chemical Biology* 9:606-12
71. Pelletier R, Danylchuk DI, Benaissa H, Broch F, Vauchelles R, et al. 2023. Genetic Targeting of Solvatochromic Dyes for Probing Nanoscale Environments of Proteins in Organelles. *Anal. Chem.* 95:8512-21
72. Garini Y, Young IT, McNamara G. 2006. Spectral imaging: Principles and applications. *Cytom. Part A* 69A:735-47
73. Gao L, Smith RT. 2015. Optical hyperspectral imaging in microscopy and spectroscopy - a review of data acquisition. *J. Biophotonics* 8:441-56
74. Favreau PF, Hernandez C, Heaster T, Alvarez DF, Rich TC, et al. 2014. Excitation-scanning hyperspectral imaging microscope. *J. Biomed. Opt.* 19:046010
75. Valm AM, Cohen S, Legant WR, Melunis J, Hershberg U, et al. 2017. Applying systems-level spectral imaging and analysis to reveal the organelle interactome. *Nature* 546:162-7
76. Chen K, Yan R, Xiang L, Xu K. 2021. Excitation spectral microscopy for highly multiplexed fluorescence imaging and quantitative biosensing. *Light Sci. Appl.* 10:97
77. Chen K, Li W, Xu K. 2022. Super-multiplexing excitation spectral microscopy with multiple fluorescence bands. *Biomed. Opt. Express* 13:6048-60
78. Wu W, Luo S, Fan C, Yang T, Zhang S, et al. 2023. Tetra-color superresolution microscopy based on excitation spectral demixing. *Light Sci. Appl.* 12:9

79. Kusumi A, Tsunoyama TA, Hirosawa KM, Kasai RS, Fujiwara TK. 2014. Tracking single molecules at work in living cells. *Nat. Chem. Biol.* 10:524-32
80. Machan R, Wohland T. 2014. Recent applications of fluorescence correlation spectroscopy in live systems. *FEBS Lett.* 588:3571-84
81. Manzo C, Garcia-Parajo MF. 2015. A review of progress in single particle tracking: from methods to biophysical insights. *Rep. Prog. Phys.* 78:124601
82. Shen H, Tauzin LJ, Baiyasi R, Wang WX, Moringo N, et al. 2017. Single particle tracking: from theory to biophysical applications. *Chem. Rev.* 117:7331-76
83. Lippincott-Schwartz J, Snapp EL, Phair RD. 2018. The Development and Enhancement of FRAP as a Key Tool for Investigating Protein Dynamics. *Biophys. J.* 115:1146-55
84. Elf J, Barkefors I. 2019. Single-molecule kinetics in living cells. *Annu. Rev. Biochem.* 88:635-59
85. Mogre SS, Brown AI, Koslover EF. 2020. Getting around the cell: physical transport in the intracellular world. *Phys Biol* 17:061003
86. Yu L, Lei Y, Ma Y, Liu M, Zheng J, et al. 2021. A Comprehensive Review of Fluorescence Correlation Spectroscopy. *Front. Phys.* 9:644450
87. Mütze J, Ohrt T, Schwille P. 2011. Fluorescence correlation spectroscopy in vivo. *Laser & Photonics Reviews* 5:52-67
88. Krieger JW, Singh AP, Bag N, Garbe CS, Saunders TE, et al. 2015. Imaging fluorescence (cross-) correlation spectroscopy in live cells and organisms. *Nature Protocols* 10:1948-74
89. Sezgin E, Schneider F, Galiani S, Urbancic I, Waithe D, et al. 2019. Measuring nanoscale diffusion dynamics in cellular membranes with super-resolution STED-FCS. *Nat. Protoc.* 14:1054-83
90. Bag N, Wohland T. 2014. Imaging Fluorescence Fluctuation Spectroscopy: New Tools for Quantitative Bioimaging. *Annual Review of Physical Chemistry* 65:225-48
91. Cognet L, Leduc C, Lounis B. 2014. Advances in live-cell single-particle tracking and dynamic super-resolution imaging. *Current Opinion in Chemical Biology* 20:78-85
92. Balzarotti F, Eilers Y, Gwosch KC, Gynnå AH, Westphal V, et al. 2017. Nanometer resolution imaging and tracking of fluorescent molecules with minimal photon fluxes. *Science* 355:606-12
93. Deguchi T, Iwanski MK, Schentarra E-M, Heidebrecht C, Schmidt L, et al. 2023. Direct observation of motor protein stepping in living cells using MINFLUX. *Science* 379:1010-5
94. Manley S, Gillette JM, Patterson GH, Shroff H, Hess HF, et al. 2008. High-density mapping of single-molecule trajectories with photoactivated localization microscopy. *Nat. Methods* 5:155-7
95. Giannone G, Hosy E, Levet F, Constals A, Schulze K, et al. 2010. Dynamic superresolution imaging of endogenous proteins on living cells at ultra-high density. *Biophys. J.* 99:1303-10
96. Shim SH, Xia C, Zhong G, Babcock HP, Vaughan JC, et al. 2012. Super-resolution fluorescence imaging of organelles in live cells with photoswitchable membrane probes. *Proc. Natl. Acad. Sci. U. S. A.* 109:13978-83
97. El Beheiry M, Dahan M, Masson JB. 2015. InferenceMAP: mapping of single-molecule dynamics with Bayesian inference. *Nat Methods* 12:594-5
98. Xiang L, Chen K, Yan R, Li W, Xu K. 2020. Single-molecule displacement mapping unveils nanoscale heterogeneities in intracellular diffusivity. *Nat. Methods* 17:524-30
99. Yan R, Chen K, Xu K. 2020. Probing nanoscale diffusional heterogeneities in cellular membranes through multidimensional single-molecule and super-resolution microscopy. *J. Am. Chem. Soc.* 142:18866-73
100. Choi AA, Xiang L, Li W, Xu K. 2023. Single-molecule displacement mapping indicates unhindered intracellular diffusion of small ($\lesssim$1 kDa) solutes. *J. Am. Chem. Soc.* 145:8510-6
101. Xiang L, Yan R, Chen K, Li W, Xu K. 2023. Single-molecule displacement mapping unveils sign-asymmetric protein charge effects on intraorganellar diffusion. *Nano Lett.* 23:1711-6
102. Moon S, Li W, Hauser M, Xu K. 2020. Graphene-enabled, spatially controlled electroporation of adherent cells for live-cell super-resolution microscopy. *ACS Nano* 14:5609-17
103. Choi AA, Park HH, Chen K, Yan R, Li W, Xu K. 2022. Displacement statistics of unhindered single molecules show no enhanced diffusion in enzymatic reactions. *J. Am. Chem. Soc.* 144:4839-44

104. Park HH, Choi AA, Xu K. 2023. Size-dependent suppression of molecular diffusivity in expandable hydrogels: A single-molecule study. *J. Phys. Chem. B* 127:3333-9
105. Śmigiel WM, Mantovanelli L, Linnik DS, Punter M, Silberberg J, et al. 2022. Protein diffusion in Escherichia coli cytoplasm scales with the mass of the complexes and is location dependent. *Sci. Adv.* 8:eabo5387
106. Tran BM, Linnik DS, Punter CM, Śmigiel WM, Mantovanelli L, et al. 2023. Super-resolving microscopy reveals the localizations and movement dynamics of stressosome proteins in Listeria monocytogenes. *Communications Biology* 6:51
107. Jameson DM, Ross JA. 2010. Fluorescence polarization/anisotropy in diagnostics and imaging. *Chem. Rev.* 110:2685-708
108. Shroder DY, Lippert LG, Goldman YE. 2016. Single molecule optical measurements of orientation and rotations of biological macromolecules. *Methods Appl. Fluoresc.* 4:042004
109. Gould TJ, Gunewardene MS, Gudheti MV, Verkhusha VV, Yin SR, et al. 2008. Nanoscale imaging of molecular positions and anisotropies. *Nat. Methods* 5:1027-30
110. Testa I, Schonle A, Middendorff CV, Geisler C, Medda R, et al. 2008. Nanoscale separation of molecular species based on their rotational mobility. *Opt. Express* 16:21093-104
111. Backer AS, Lee MY, Moerner WE. 2016. Enhanced DNA imaging using super-resolution microscopy and simultaneous single-molecule orientation measurements. *Optica* 3:659-66
112. Valades Cruz CA, Shaban HA, Kress A, Bertaux N, Monneret S, et al. 2016. Quantitative nanoscale imaging of orientational order in biological filaments by polarized superresolution microscopy. *Proc. Natl. Acad. Sci. U. S. A.* 113:E820-E8
113. Backer AS, Biebricher AS, King GA, Wuite GJL, Heller I, Peterman EJG. 2019. Single-molecule polarization microscopy of DNA intercalators sheds light on the structure of S-DNA. *Sci Adv* 5:eaav1083
114. Mehta SB, McQuilken M, La Riviere PJ, Occhipinti P, Verma A, et al. 2016. Dissection of molecular assembly dynamics by tracking orientation and position of single molecules in live cells. *Proc. Natl. Acad. Sci. U. S. A.* 113:E6352-E61
115. Rimoli CV, Valades-Cruz CA, Curcio V, Mavrakis M, Brasselet S. 2022. 4polar-STORM polarized super-resolution imaging of actin filament organization in cells. *Nature Communications* 13:301
116. Lu J, Mazidi H, Ding T, Zhang O, Lew MD. 2020. Single-molecule 3D orientation imaging reveals nanoscale compositional heterogeneity in lipid membranes. *Angew. Chem. Int. Ed.* 59:17572-9
117. Zhang O, Guo Z, He Y, Wu T, Vahey MD, Lew MD. 2023. Six-dimensional single-molecule imaging with isotropic resolution using a multi-view reflector microscope. *Nature Photonics* 17:179-86
118. Berezin MY, Achilefu S. 2010. Fluorescence lifetime measurements and biological imaging. *Chem. Rev.* 110:2641-84
119. Sarder P, Maji D, Achilefu S. 2015. Molecular Probes for Fluorescence Lifetime Imaging. *Bioconjugate Chemistry* 26:963-74
120. Rupsa D, Tiffany MH, Joe TS, Amani AG, Melissa CS. 2020. Fluorescence lifetime imaging microscopy: fundamentals and advances in instrumentation, analysis, and applications. *J. Biomed. Opt.* 25:071203
121. Thiele JC, Helmerich DA, Oleksiievets N, Tsukanov R, Butkevich E, et al. 2020. Confocal fluorescence-lifetime single-molecule localization microscopy. *ACS Nano* 14:14190-200
122. Oleksiievets N, Mathew C, Thiele JC, Gallea JI, Nevskyi O, et al. 2022. Single-Molecule Fluorescence Lifetime Imaging Using Wide-Field and Confocal-Laser Scanning Microscopy: A Comparative Analysis. *Nano Letters* 22:6454-61
123. Bowman AJ, Kasevich MA. 2021. Resonant Electro-Optic Imaging for Microscopy at Nanosecond Resolution. *ACS Nano* 15:16043-54
124. Masullo LA, Steiner F, Zähringer J, Lopez LF, Bohlen J, et al. 2021. Pulsed Interleaved MINFLUX. *Nano Letters* 21:840-6
125. Zaza C, Chiarelli G, Zweifel LP, Pilo-Pais M, Sisamakis E, et al. 2023. Super-Resolved FRET Imaging by Confocal Fluorescence-Lifetime Single-Molecule Localization Microscopy. *Small Methods*:2201565

126. Thiele JC, Jungblut M, Helmerich DA, Tsukanov R, Chizhik A, et al. 2022. Isotropic three-dimensional dual-color super-resolution microscopy with metal-induced energy transfer. *Science Advances* 8:eabo2506
127. Zähringer J, Cole F, Bohlen J, Steiner F, Kamińska I, Tinnefeld P. 2023. Combining pMINFLUX, graphene energy transfer and DNA-PAINT for nanometer precise 3D super-resolution microscopy. *Light: Science & Applications* 12:70
128. Arroyo JO, Kukura P. 2015. Non-fluorescent schemes for single-molecule detection, imaging and spectroscopy. *Nat. Photonics* 10:11-7
129. Leighton RE, Alperstein AM, Frontiera RR. 2022. Label-Free Super-Resolution Imaging Techniques. *Annual Review of Analytical Chemistry* 15:37-55
130. Tang M, Han Y, Jia D, Yang Q, Cheng J-X. 2023. Far-field super-resolution chemical microscopy. *Light: Science & Applications* 12:137
131. Wang G, Stender AS, Sun W, Fang N. 2010. Optical imaging of non-fluorescent nanoparticleprobes in live cells. *The Analyst* 135:215-21
132. Adhikari S, Spaeth P, Kar A, Baaske MD, Khatua S, Orrit M. 2020. Photothermal Microscopy: Imaging the Optical Absorption of Single Nanoparticles and Single Molecules. *ACS Nano* 14:16414-45
133. Young G, Kukura P. 2019. Interferometric scattering microscopy. *Annu. Rev. Phys. Chem.* 70:301-22
134. Taylor RW, Mahmoodabadi RG, Rauschenberger V, Giessl A, Schambony A, Sandoghdar V. 2019. Interferometric scattering microscopy reveals microsecond nanoscopic protein motion on a live cell membrane. *Nature Photonics* 13:480-7
135. Priest L, Peters JS, Kukura P. 2021. Scattering-based Light Microscopy: From Metal Nanoparticles to Single Proteins. *Chem. Rev.* 121:11937-70
136. Dahmardeh M, Mirzaalian Dastjerdi H, Mazal H, Köstler H, Sandoghdar V. 2023. Self-supervised machine learning pushes the sensitivity limit in label-free detection of single proteins below 10 kDa. *Nat. Methods* 20:442-7
137. Zipfel WR, Williams RM, Webb WW. 2003. Nonlinear magic: multiphoton microscopy in the biosciences. *Nature Biotechnology* 21:1369-77
138. Min W, Freudiger CW, Lu S, Xie XS. 2011. Coherent Nonlinear Optical Imaging: Beyond Fluorescence Microscopy. *Annual Review of Physical Chemistry* 62:507-30
139. Parodi V, Jacchetti E, Osellame R, Cerullo G, Polli D, Raimondi MT. 2020. Nonlinear Optical Microscopy: From Fundamentals to Applications in Live Bioimaging. *Front Bioeng Biotechnol* 8:585363
140. Qian C, Miao K, Lin L-E, Chen X, Du J, Wei L. 2021. Super-resolution label-free volumetric vibrational imaging. *Nat. Commun.* 12:3648
141. Shi L, Klimas A, Gallagher B, Cheng Z, Fu F, et al. 2022. Super-Resolution Vibrational Imaging Using Expansion Stimulated Raman Scattering Microscopy. *Advanced Science* 9:2200315
142. Xiong H, Qian N, Miao Y, Zhao Z, Chen C, Min W. 2021. Super-resolution vibrational microscopy by stimulated Raman excited fluorescence. *Light Sci. Appl.* 10:87
143. Steves MA, Knappenberger KL. 2023. Improving Spectral, Spatial, and Mechanistic Resolution Using Fourier Transform Nonlinear Optics: A Tutorial Review. *ACS Physical Chemistry Au* 3:130-42
144. Wang M, Li M, Jiang S, Gao J, Xi P. 2020. Plasmonics meets super-resolution microscopy in biology. *Micron* 137:102916
145. Zrimsek AB, Chiang N, Mattei M, Zaleski S, McAnally MO, et al. 2017. Single-Molecule Chemistry with Surface- and Tip-Enhanced Raman Spectroscopy. *Chemical Reviews* 117:7583-613
146. Itoh T, Procházka M, Dong Z-C, Ji W, Yamamoto YS, et al. 2023. Toward a New Era of SERS and TERS at the Nanometer Scale: From Fundamentals to Innovative Applications. *Chemical Reviews* 123:1552-634
147. Ayas S, Cinar G, Ozkan AD, Soran Z, Ekiz O, et al. 2013. Label-Free Nanometer-Resolution Imaging of Biological Architectures through Surface Enhanced Raman Scattering. *Scientific Reports* 3:2624
148. Olson AP, Ertsgaard CT, Elliott SN, Lindquist NC. 2016. Super-Resolution Chemical Imaging with Plasmonic Substrates. *ACS Photonics* 3:329-36

149. Hauser M, Wojcik M, Kim D, Mahmoudi M, Li W, Xu K. 2017. Correlative super-resolution microscopy: new dimensions and new opportunities. *Chem. Rev.* 117:7428-56

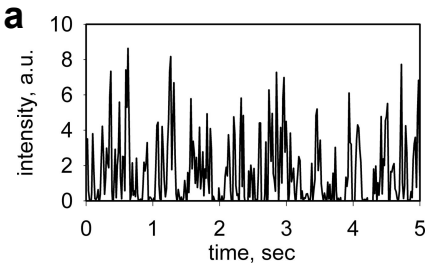
a
intensity, a.u.
time, sec
0
2
4
6
8
10
0
1
2
3
4
5

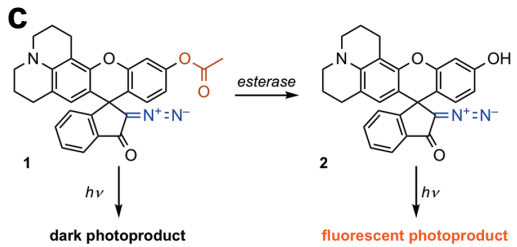
c
esterase
1
2
hν
hν
dark photoproduct
fluorescent photoproduct

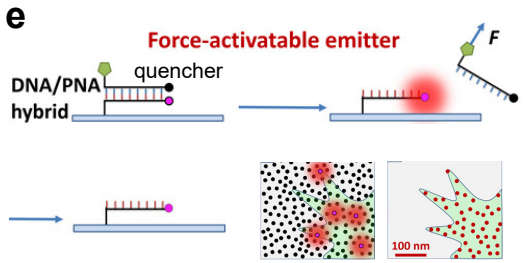
e
Force-activatable emitter
F
DNA/PNA
hybrid
quencher
100 nm

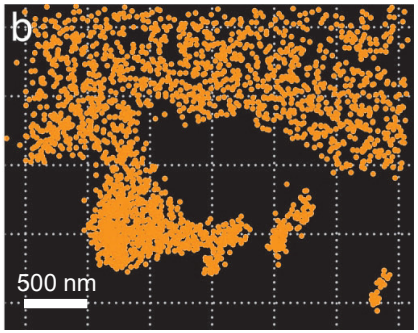
b
500 nm

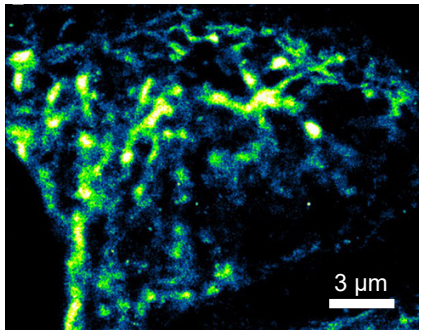
d
3 μm

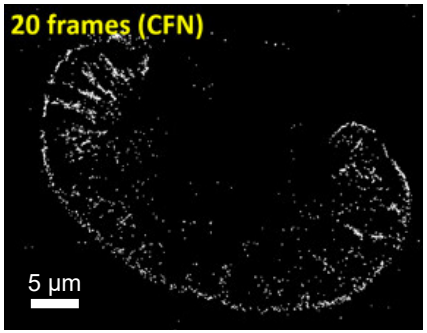
f
20 frames (CFN)
5 μm

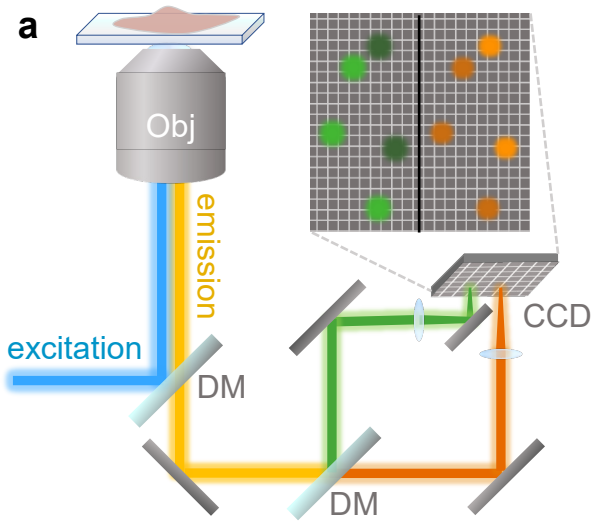
a
Obj
emission
excitation
DM
DM
CCD

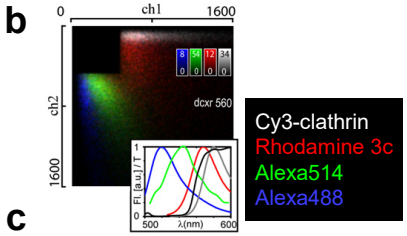
b
ch1
1600
0
ch2
1600
dcxr 560
Fl. [a.u.] / T
500
λ(nm)
600
Cy3-clathrin
Rhodamine 3c
Alexa514
Alexa488

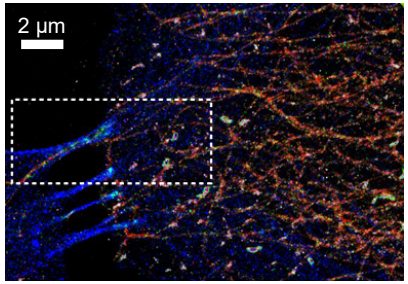
c
2 µm

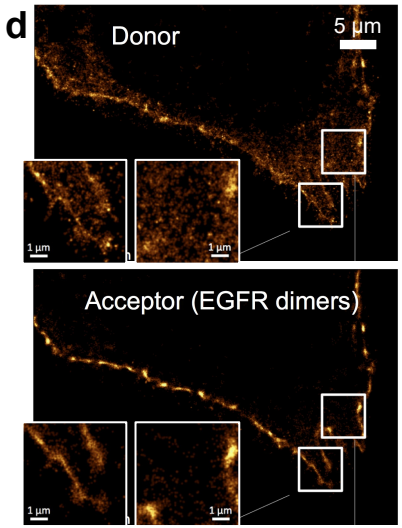
d
Donor
5 µm
1 µm
1 µm
Acceptor (EGFR dimers)
1 µm
1 µm

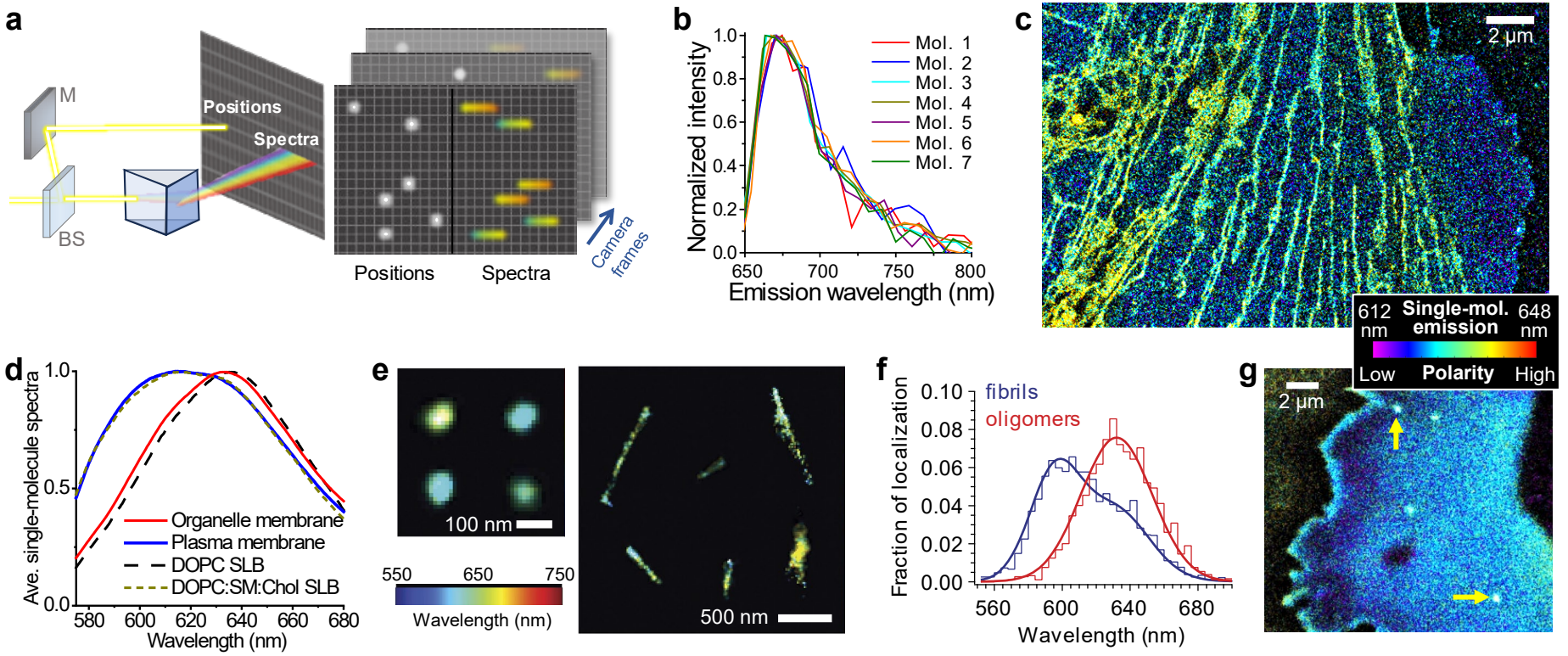
a
M
BS
Positions
Spectra
Positions
Spectra
Camera frames
b
Normalized intensity
Emission wavelength (nm)
Mol. 1
Mol. 2
Mol. 3
Mol. 4
Mol. 5
Mol. 6
Mol. 7
c
2 µm
612 nm
Single-mol. emission
648 nm
Low
Polarity
High
d
Ave. single-molecule spectra
Wavelength (nm)
Organelle membrane
Plasma membrane
DOPC SLB
DOPC:SM:Chol SLB
e
100 nm
550
650
750
Wavelength (nm)
500 nm
f
Fraction of localization
Wavelength (nm)
fibrils
oligomers
g
2 µm

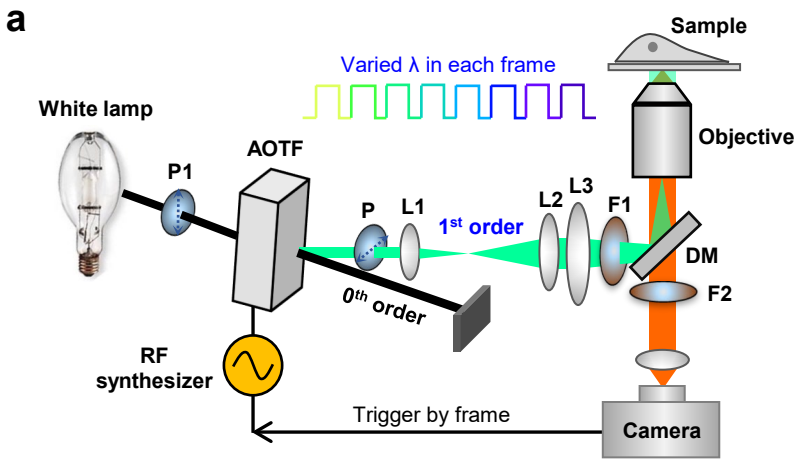
a
Sample
Varied λ in each frame
White lamp
Objective
AOTF
P1
P
L1
1st order
L2
L3
F1
DM
F2
0th order
RF synthesizer
Trigger by frame
Camera

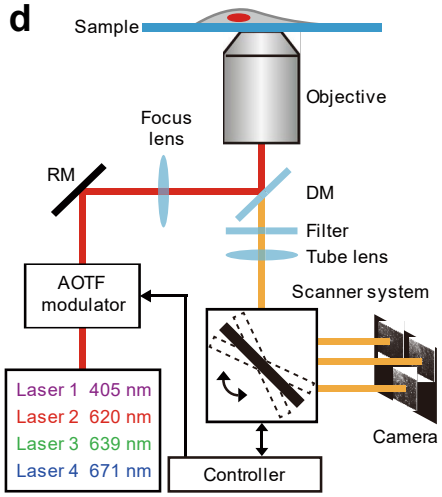
d
Sample
Objective
Focus lens
RM
DM
Filter
Tube lens
Scanner system
AOTF modulator
Laser 1 405 nm
Laser 2 620 nm
Laser 3 639 nm
Laser 4 671 nm
Controller
Camera

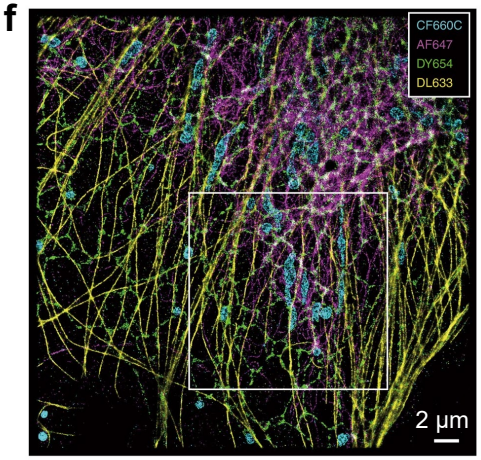
f
CF660C
AF647
DY654
DL633
2 μm

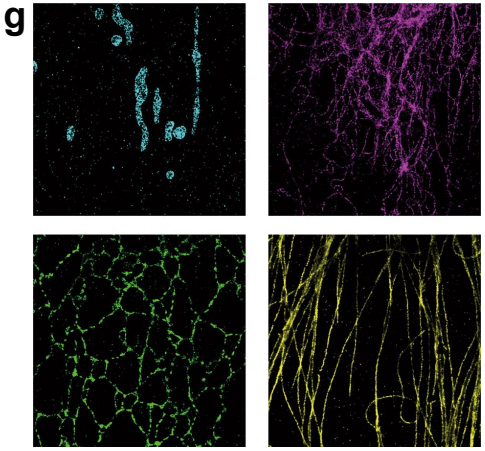
g

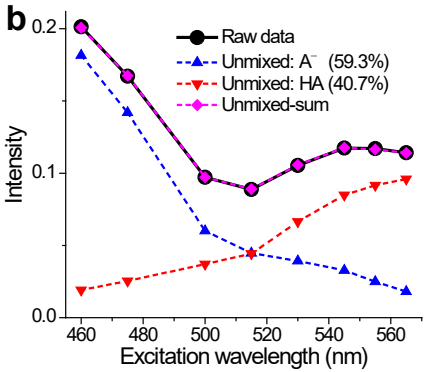
b
Raw data
Unmixed: A⁻ (59.3%)
Unmixed: HA (40.7%)
Unmixed-sum
Intensity
Excitation wavelength (nm)

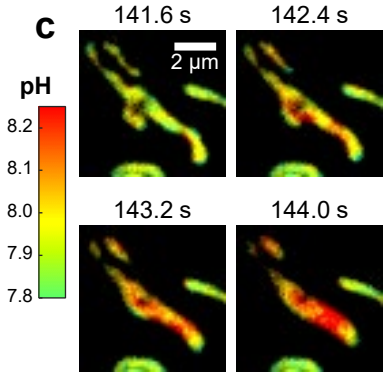
c
pH
141.6 s
142.4 s
143.2 s
144.0 s
2 μm

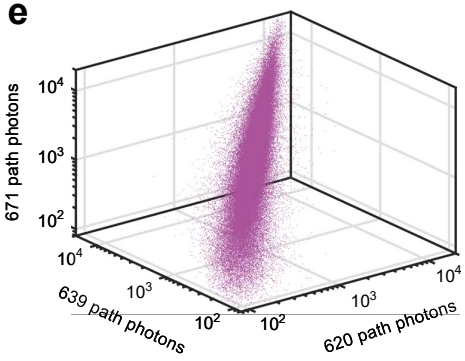
e
671 path photons
639 path photons
620 path photons

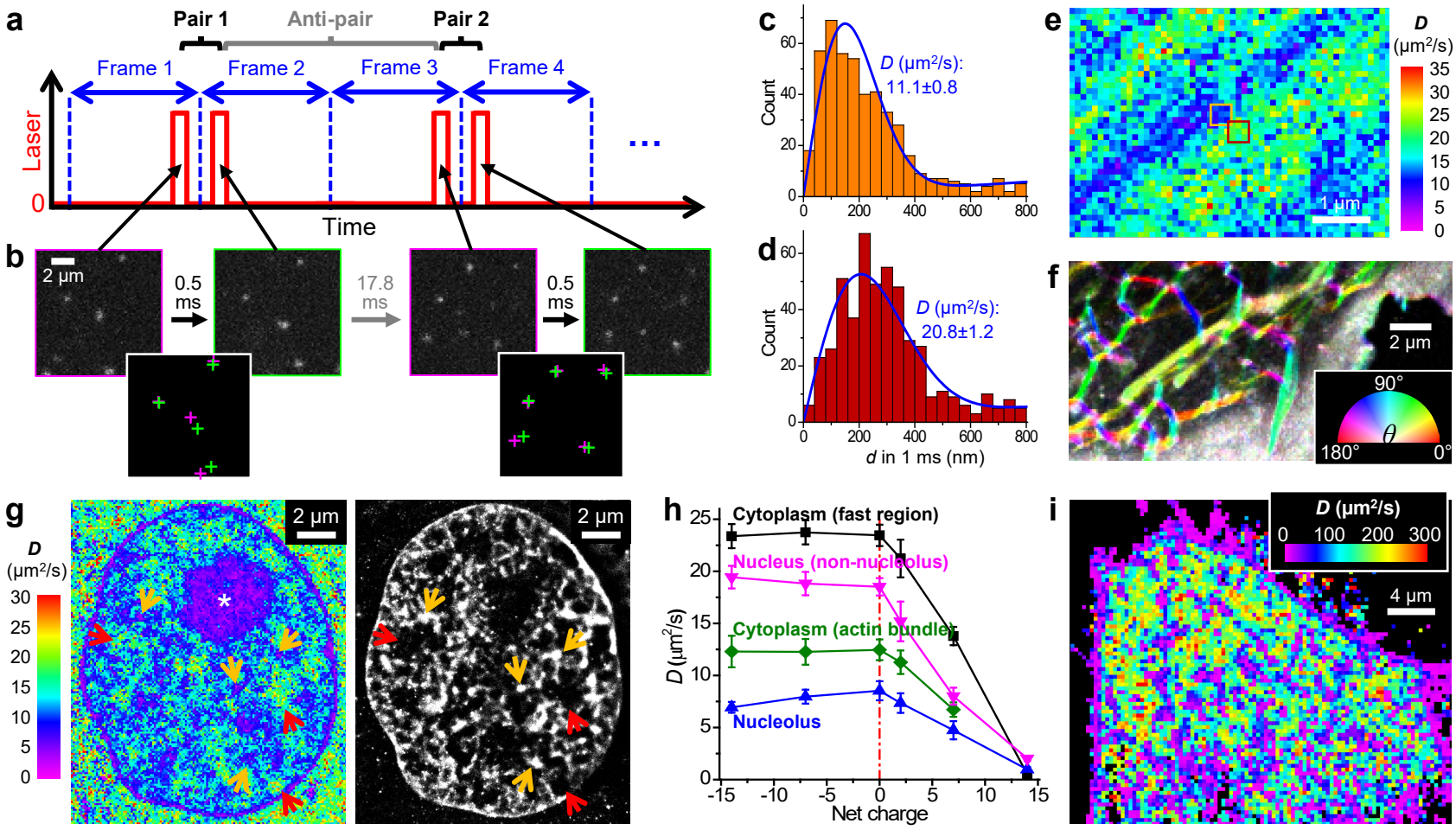
a
Pair 1
Anti-pair
Pair 2
Frame 1
Frame 2
Frame 3
Frame 4
Laser
0
Time
b
2 μm
0.5 ms
17.8 ms
0.5 ms
c
Count
D (μm²/s): 11.1±0.8
d
Count
D (μm²/s): 20.8±1.2
d in 1 ms (nm)
e
D (μm²/s)
1 μm
f
2 μm
90°
θ
180°
0°
g
D (μm²/s)
2 μm
2 μm
h
Cytoplasm (fast region)
Nucleus (non-nucleolus)
Cytoplasm (actin bundle)
Nucleolus
D (μm²/s)
Net charge
i
D (μm²/s)
4 μm

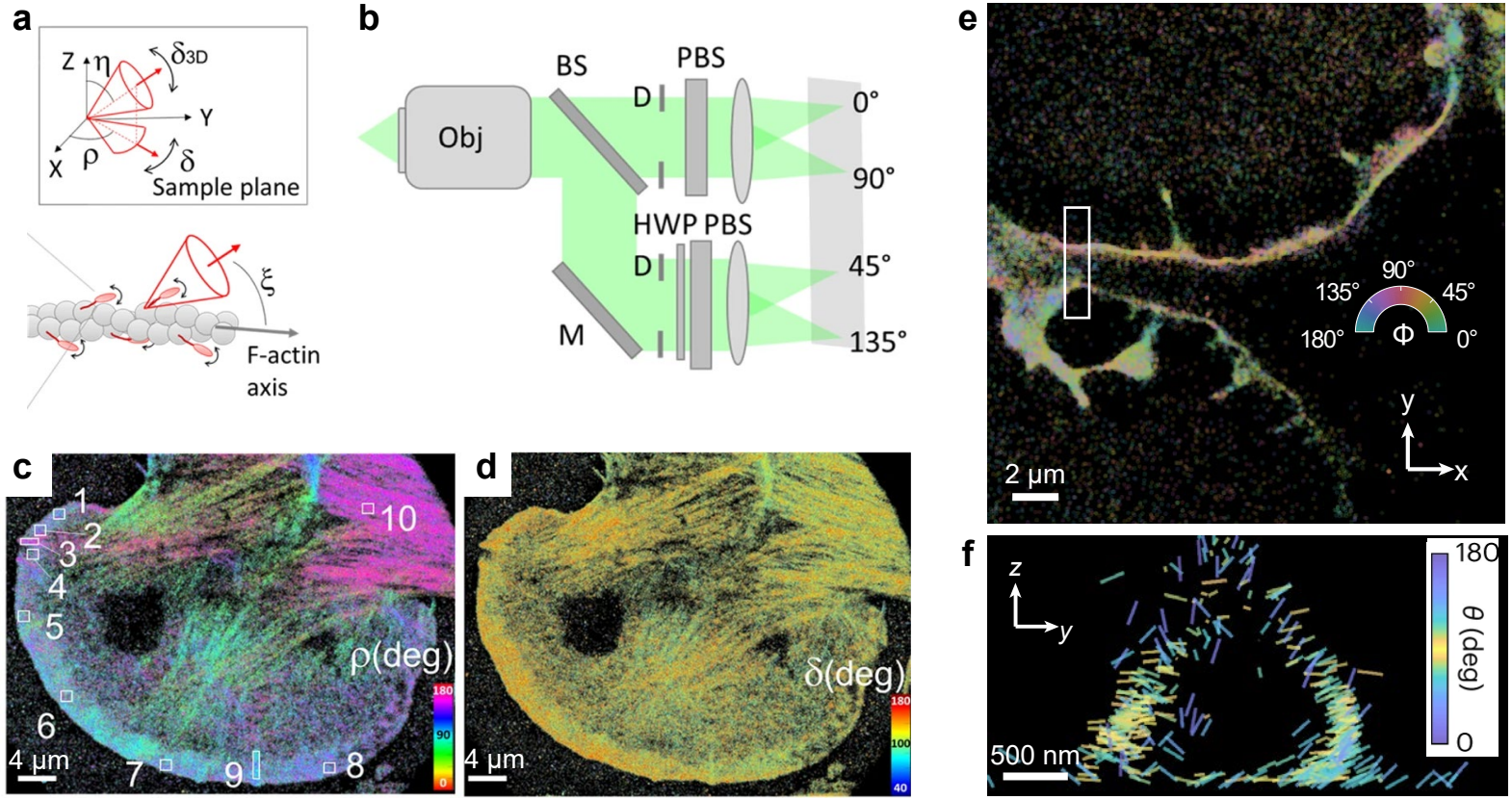
a
Z
η
δ3D
Y
X
ρ
δ
Sample plane
ξ
F-actin
axis
b
Obj
BS
PBS
D
0°
90°
HWP
PBS
D
45°
M
135°
c
1
2
3
4
5
6
7
9
8
10
ρ(deg)
180
90
0
4 μm
d
δ(deg)
180
100
40
4 μm
e
90°
135°
45°
180°
Φ
0°
y
x
2 μm
f
z
y
180
θ (deg)
0
500 nm

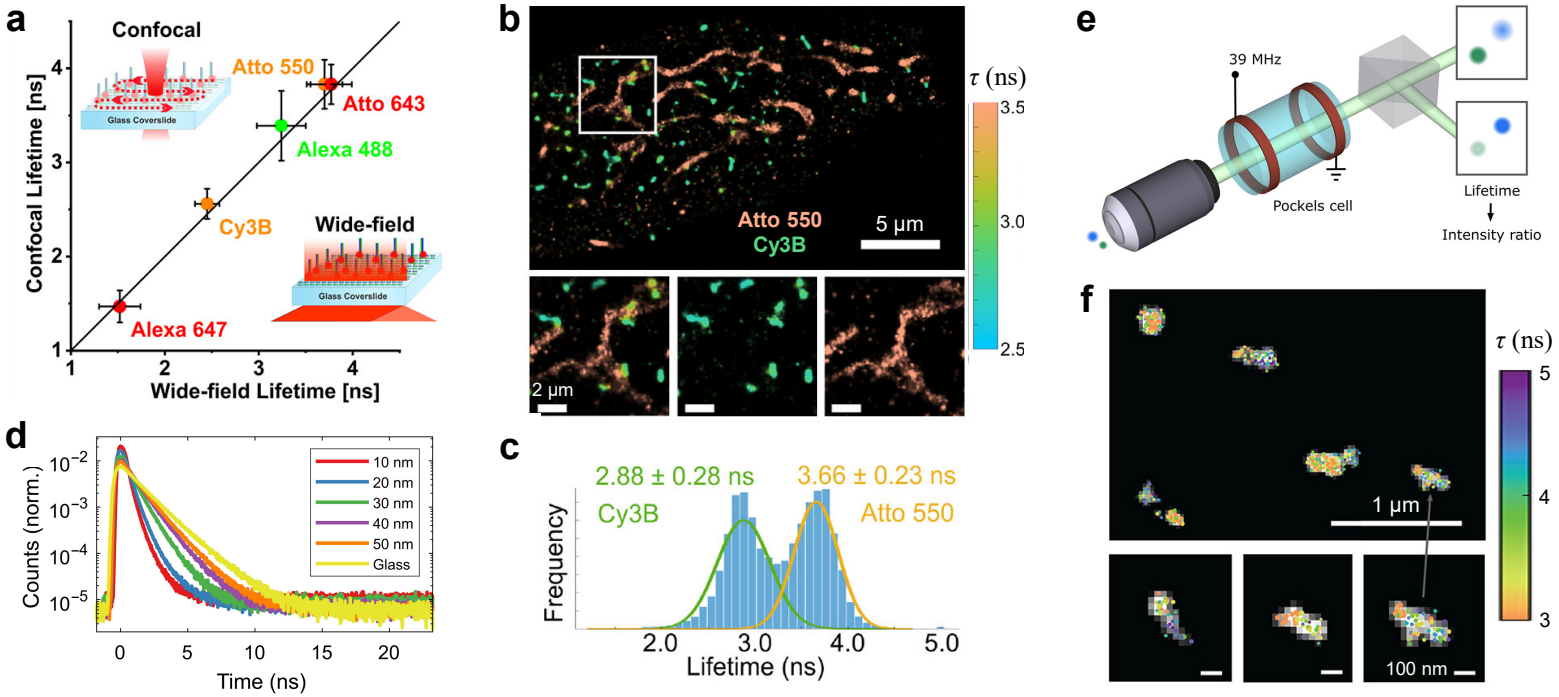
a
Confocal
Atto 550
Atto 643
Alexa 488
Cy3B
Wide-field
Alexa 647
Glass Coverslide
Confocal Lifetime [ns]
Wide-field Lifetime [ns]
b
Atto 550
Cy3B
5 µm
2 µm
τ (ns)
3.5
3.0
2.5
c
2.88 ± 0.28 ns
Cy3B
3.66 ± 0.23 ns
Atto 550
Frequency
Lifetime (ns)
d
10 nm
20 nm
30 nm
40 nm
50 nm
Glass
Counts (norm.)
Time (ns)
e
39 MHz
Pockels cell
Lifetime
Intensity ratio
f
1 µm
100 nm
τ (ns)
5
4
3